J. Appl. Comput. Mech., xx(x) (2026) 1-13
DOI: 10.22055/jacm.2026.49256.5843

ISSN: 2383-4536
jacm.scu.ac.ir

Shahid Chamran University of Ahvaz

Journal of Applied and Computational Mechanics

Research Paper

Advanced Heat Sink Fin Design: A Study on Geometric Parameters and Their Influence on Convective Heat Transfer for Double-Pass Solar Photovoltaic Thermal (PVT)

Lin Hai Yang[1], Muhammad Amir Aziat Ishak[2], Nurul 'Atiqah Bt Ahmad[1], Zikrul Hakiem[3]

[1] School of Engineering, Faculty of Innovation & Technology, Taylor's University, Lakeside Campus, Subang Jaya, Selangor, Malaysia, Email: linhaiyang764@gmail.com (L.H.Y); NurulAtiqah.Ahmad@taylors.edu.my (N.A.B.A)

[2] Solar Energy Research Institute, Universiti Kebangsaan Malaysia, 43600 Bangi, Selangor, Malaysia. Email: amir.ishak@ukm.edu.my

[3] Faculty of Industrial Management, Universiti Malaysia Pahang, 26300 Kuantan, Pahang, Malaysia. Email: zikrul@umpsa.edu.my

Received April 12 2026; Revised May 25 2026; Accepted for publication May 27 2026.
✉ Corresponding author: M.A.A. Ishak (amir.ishak@ukm.edu.my)

Abstract. A photovoltaic–thermal (PVT) collector is a hybrid system capable of generating electrical and thermal energy simultaneously. However, the efficiency of photovoltaic (PV) modules decreases with rising operating temperature, limiting overall system performance. This study focuses on enhancing the performance of a PVT system by integrating a heat-sink fin collector with improved geometrical designs. The proposed heat sink has dimensions of 400 × 400 mm with a 10 mm edge spacing and a fin length of 5 cm, incorporating repeating fin patterns to maximize heat dissipation. By increasing the surface area, the heat sink absorbs excess heat from the PV module, reducing its operating temperature and improving electrical efficiency while recovering useful thermal energy. Five different fin designs were developed and evaluated using computational fluid dynamics (CFD) analysis under airflow ranging from 2 m/s to 10 m/s, with solar irradiance between 600 and 100 W/m^2. Both electrical and thermal efficiencies were analyzed and compared to identify the most effective design. The results show that Design 1 achieved the highest overall efficiency, with efficiency ranging from 49.02% to 66.58% under constant irradiance of 100 W/m^2. The photovoltaic efficiency was 13.3%, while thermal efficiency exceeded 53% at the highest flow rate. Furthermore, increasing airflow velocity reduces the PV temperature from 43°C to 30°C, improving electrical performance. The findings show that the optimum heat sink geometry significantly improves heat transfer and overall performance of the double-pass PVT system.

Keywords: Photovoltaic thermal, Electrical energy, Thermal energy, Heat dissipation, Heat sink, Fins.

1. Introduction

Solar energy has always been a viable source of energy when it comes to renewable energy sources, but it has only gained more attention in recent years. One common type of solar panel utilizes photovoltaic cells to generate power [1-3], but photovoltaic modules have a major downside. As the solar panel operates and the PVT is exposed to solar irradiance, the temperature of the PVT increases, and the module's efficiency declines [4-6]. Therefore, a cooling system is essential in boosting the efficiency of the module, and installing heat sink fins is one of the many viable ways of improving the heat dissipation rate. Although several PVT studies have been conducted so far, a design of optimized fins which simultaneously maximizes the thermal performance and reduces the pressure drop and material consumption of the PVT system still needs to be developed [7-10]. This project aims to design, evaluate, and analyze the performance of PVT collectors with various CFD-simulated heat-sink fin designs.

In 2018, Zawiwi et al. [11] provided an in-depth review of the fundamentals of computational fluid dynamics. In this review, it is stated that the mathematical equations describing the fluid flow are first written, the domain is then divided into smaller elements, and these initial and boundary conditions are utilized to solve these equations and simulate the realistic behavior of physical models. In 2025, Ahmed et al. [12] investigated photovoltaic thermal module efficiency through optimization of heat sink designs in Jeddah, Saudi Arabia, and the results of Ahmed et al's research show that the proposed heat sink design can improve photovoltaic efficiency by 14.019%, and relatively enhance the efficiency by 70.10%, as well as reducing the maximum surface temperature of the solar cell by 30% at an air velocity of 2.5m/s.

In 2022, Pathak et al. [13] conducted research surrounding the performance of PVT systems utilizing various cooling methods, including jet impingement, airflow cooling, immersion cooling with liquids, and many more. The performance of each cooling method was evaluated based on the overall efficiency of the PVT system, including the use of heat sinks as a passive cooling mechanism. In 2023, Pujol et al. [14] had research surrounding the design of plate-fin heat sinks that are utilized for single-module thermoelectric generators, and based on results obtained from their research, it was concluded that the optimal heat sink designs had fin thicknesses of 0.32 and 0.44 mm, with fin-to-fin distances of 1 mm. Although in this experiment the heat sink fins were utilized for a different application, the conclusion relating to the optimal fin thickness and fin-to-fin distance is still very useful information that can be utilized in the design of heat sink fins for solar photovoltaic cells.

In 2022, Khudhur et al. [15] conducted research on the thermal analysis of heat transfer with different fin geometries and had multiple key findings. Firstly, they found heat sinks with add- and subtract-shaped fins more effective than straight fins in terms of heat dissipation rate. Secondly, as the heat flux increases, the heat transfer coefficient and Nusselt number increase for all heat-sink types for constant Reynolds number. In 2024, Harris et al. [16] researched the heat transfer optimization of novel biomorphic pin-fin heat sinks, where the unconventional design proposed by this paper was able to save from 6.3% to 14.3% of material usage while still producing around 1.5 ~ 1.7 times more heat transfer. The proposed design showed that sometimes jumping out of the box when designing can yield very surprising results. However, it is also important to consider its manufacturing complexity when it comes to mass production, which may explain why these unconventional designs are not applied more widely. In summary, although PVT collector systems could theoretically reach upward of 60 ~ 80% in overall efficiency, the efficiency drastically drops as the inlet temperature rises, therefore, efficient heat dissipation is critical to maintain high overall efficiency throughout the operation, it was also confirmed by Chander et al. [17, 18] that the efficiency of monocrystalline silicon solar cells, the type of solar cell used in this research, decreases as the cell temperature increases.

In this work, five different geometrical heat sink fin configurations are proposed specifically for double-pass PVT applications, unlike the conventional straight-fin or uniform pin-fin configurations reported in previous PVT studies. The novelty of the present study is the comparative study of slanted flat-plate fins, thin pin fins, short flat-plate fins, perforated flat-plate fins, and X-shaped flat-plate arrangements under identical CFD operating conditions. The purpose of the geometrical modifications was to improve the airflow and system interaction, increase the effective heat-transfer surface area, minimize thermal storage, and maximize the overall PVT performance (both PV and thermal). In addition, novel fin configurations are implemented into the double-pass airflow configuration to understand passive thermal management techniques for solar PVT systems. This study aims to determine the best design of the heat sink fins to have the highest electrical efficiency for the PVT collector and the highest thermal efficiency for the heat sink. Initially, the simulation is performed under a constant maximum solar irradiance of 1000 W/m^2, and the performance evaluation of each geometrical shape design is done under this constant solar irradiance to determine the best-performing geometrical design. To avoid methodological redundancy, only the best-performing design will be tested by varying solar irradiance. Since the entire project uses CFD, the data and results may differ from practical applications. For this research study, the parameters analyzed are as follows: solar irradiance, air mass flow rate, air velocity, photovoltaic cell temperature, and air outlet temperature. By comparing these parameters, their relationship can be found, and the performance of each solar photovoltaic collector's heat-sink fin design can be evaluated. However, this project only investigates the effect of heat sink fin design on the photovoltaic cell's electrical efficiency and the heat-sink fin's thermal efficiency. The five designs all use the same material to ensure consistency in analysis. In this case, the material used is aluminum.

2. Methodology

2.1. Geometry

For this project, ANSYS Fluent is used to simulate airflow and obtain data regarding the electrical and thermal performances of each design. To conduct CFD analysis for each of the five geometrical designs of heat sink fins utilized in the solar photovoltaic thermal collector system, each design must first be prepared in ANSYS DesignModeler to ensure smooth simulation. The heat sink is positioned on the top of a 40cm x 40cm x 18cm box that represents the PVT collector system with the heat sink fins facing downwards, a separator is positioned at the middle of the PVT system to separate the inlet and outlet, and the Boolean subtract function is used to separate the heat sink, separator and the air domain into individual parts, with the material property of the air domain being changed into fluid for further simulation. Figure 1 shows a schematic illustration of the double-pass PVT collector, while Fig. 2 displays the geometric designs that correspond to each of the five designs tested. These designs are inspired by literature reviews, in which certain features have shown high photovoltaic and thermal efficiency. For example, design 1 is inspired by Gaikwad et al.'s research [19] where they tested out a staggered plate fin array arrangement, and design 4 is inspired by Al-Damook et al.'s research [20] where it was discovered that a heat sink could have higher overall performance with perforations through the fins. The various fin geometries were intentionally developed to enhance convective heat transfer under different airflow obstructions and surface exposure to explore their influence on convective heat transfer enhancement within the double-pass PVT collector. The proposed configurations are designed to enhance thermal dissipation capability compared to conventional straight-fin heat sinks while being manufacturable. The proposed heat sink configurations are novel because they involve changes in flow paths and localized turbulence effects that can improve thermal dissipation capability without compromising manufacturability. This study is also unique in its use of perforated and X-shaped fin arrangements, which are uncommon geometries used in solar photovoltaic thermal collector applications.

In simulating the complete PVT collector system in ANSYS, solar irradiance would be applied to the top plane of the model to simulate the PV module receiving solar irradiance and dissipating heat into the thermal collector. This thermal collector is a double-pass design. Cold air enters the inlet at the top of the system along the heat sink fins, where heat dissipates into the cold air. The cold air then passes through the channel, along the lower half of the system, and exits through the outlet.

2.2. Mesh independent study

Once the geometry is completed in Design Modeler, meshing can be done on the design. Adaptive mesh sizing is used in this simulation to automatically refine the mesh in critical areas and obtain good solution accuracy without extensive manual effort for each custom sizing. Each adaptive mesh size (ranging from 1 to 7) is tested, and the number of nodes and elements, average element quality, skewness, and orthogonal quality are recorded for each resolution. Once all mesh sizes have been tested, the performance of each resolution is compared to the best-performing resolution for the design, and this process is repeated for all five geometrical designs, shown in Fig. 3, Fig. 4, and Table 1.

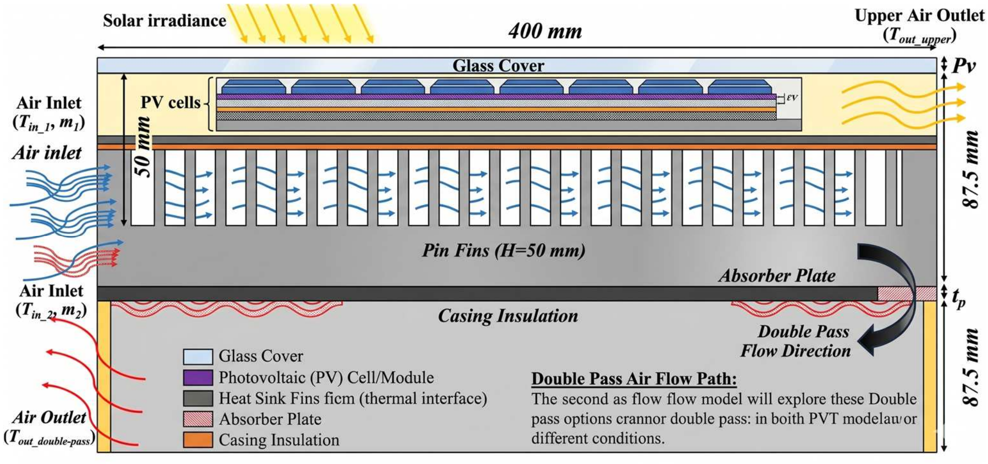

Fig. 1. Schematic diagram of the double-pass PVT collector.

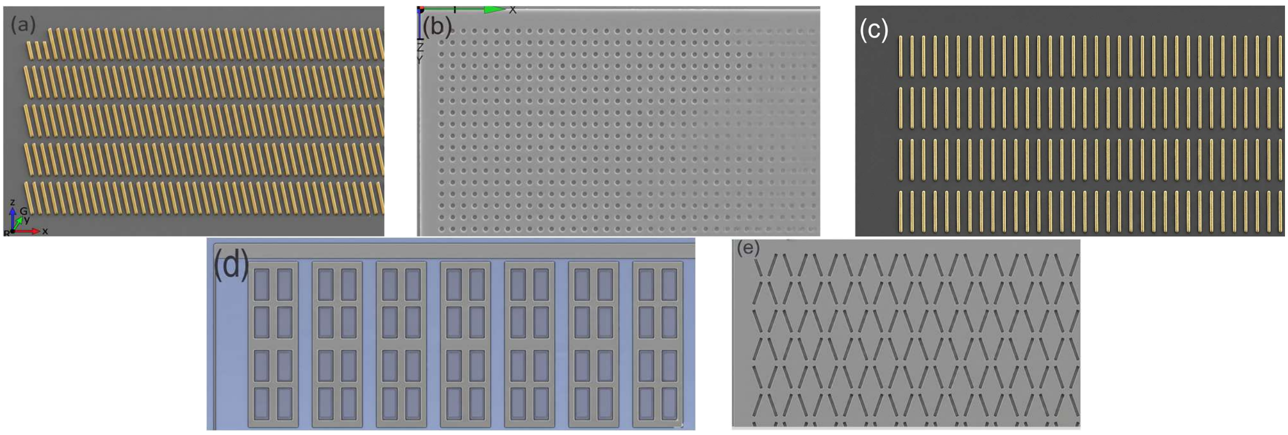

Fig. 2. Different geometry designs starting from top left, (a) Design 1 [slanted flat plate], (b) Design 2 [thin pins], (c) Design 3 [short flat plates], (d) Design 4 [flat plate with perforations] and, (e) Design 5 [x-shaped flat plate arrangement].

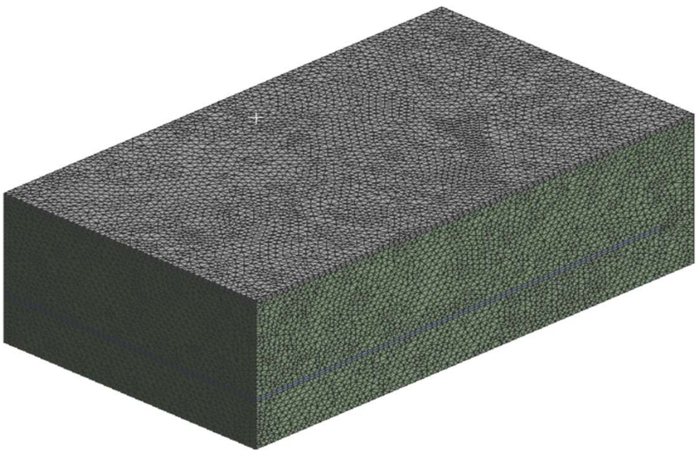

Fig. 3. Sample meshing in ANSYS meshing (Design 1, adaptive sizing 7).

Table 1. Sample mesh independent study (Design 1).

Mesh	Average Element Quality	No of Element	Skewness	Orthogonal
Extra coarse (1)	0.47455	494,207	0.661	0.337
Coarser (2)	0.49478	515,770	0.630	0.368
Coarse (3)	0.62075	714,630	0.580	0.418
Normal (4)	0.64422	1,239,819	0.537	0.462
Fine (5)	0.68491	1,753,107	0.468	0.530
Finer (6)	0.72865	3,644,925	0.397	0.601
extra fine (7)	0.74354	4,817,869	0.330	0.668

Table 2. Validation results.

Mass Flow Rate (kg/s)	Yusaidi et al. [21]	Current Work	Error (%)
0.014	51.71	52.85	2.15
0.016	53.74	54.75	1.85
0.018	55.26	56.65	2.45
0.025	59.91	61.35	2.35
0.035	63.81	65.55	2.65
Average percentage error (%)			2.29%
Average percentage accuracy (%)			97.71%

Based on the results and observations in Table 1, as adaptive mesh sizing increases, the complexity of the model's meshing increases, indicated by both the number of nodes and elements. As the model's complexity increases, improvements in average element quality, skewness, and orthogonal quality can also be observed by increasing mesh size. Extra-fine meshing has the highest average elemental and orthogonal quality and the lowest skewness compared to other mesh sizes. Therefore, extra-fine mesh sizing is used in the simulation of the five designs to ensure that the CFD analysis' results are as accurate and precise as possible. After the best-performing adaptive mesh sizing resolution has been determined and completed, named selections need to be created to assign specific geometry contours as the inlet, outlet, and PV module, allowing the definition of boundary conditions in ANSYS Fluent on these named contours.

2.3. Validation of setup

Using the same boundary conditions and settings, modelling and experimental results from Yusaidi et al. [21] were used to validate the setup. Results from this simulation are compared with previous data to evaluate setup reliability, ensuring the simulation setup's results are as accurate and reliable as possible. Validation results are shown in Table 2. As seen in the table, there is an error in the results. However, this error is not significant enough to affect the result obtained through simulation. Figure 5 visualizes the comparison between the current work and the results from Yusaidi et al. [21].

2.4. Parameters and boundary conditions

With all named selection contours defined, the next step in the CFD simulation is to calculate all relevant data with ANSYS Fluent. All options are left as is in the ANSYS Fluent setup interface, except for adding Double Precision and 8 Parallel Solver Processes to speed up the simulation. In ANSYS Fluent, the energy equation in "Models" section is turned on to solve for the conservation of energy and calculate the temperature of the fluid, which in this case is flowing air, as for the boundary equation, the velocity magnitude of air at the inlet is set to range from 2 m/s to 10 m/s with intervals of 2 m/s, and the solar irradiance applied to the PV Module is fixed at 1000 W/m^2, with the remaining settings left as default.

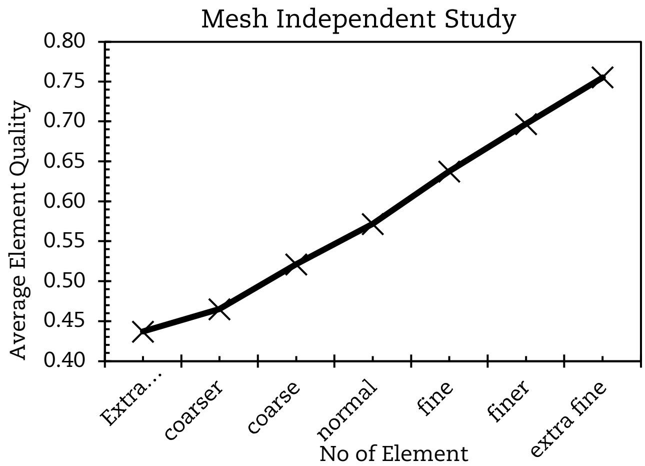

Fig. 4. Sample mesh independence study graph in Microsoft Excel (Design 1).

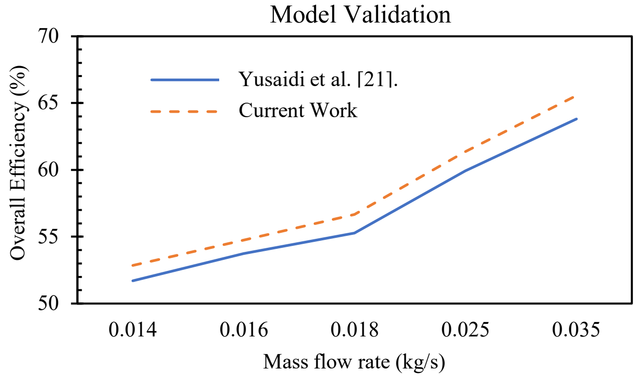

Fig. 5. Comparison between the current work and Yusaidi et al. [21].

Table 3. Parameters and base values of independent variables.

Parameter	Value
Air flow rate, V	2 m/s – 10 m/s
Solar irradiance, I	1000 W/m^2
Ambient temperature, T_a	30 °C
Area of collector, A_c	0.052 m^2
Cross-sectional area of collector, A	0.072 m^2
Density of air, ρ	1.16 kg/m^3
Width of collector, W	400 mm
Depth of collector, d	87.5 mm
PV temperature coefficient, α_{PV}	0.91
Packing factor, P	0.90
Reflectivity of jet plate, n_r	0.70
Optical transmittance, τ_i	0.85
Temperature coefficient, β	0.0045 K^{-1}
Temperature at reference condition, T_{ref}	303.15 K
Electrical efficiency at reference condition, η_{ref}	0.16
Inlet temperature, T_i	27 °C

Table 3 presents the parameters and base values used in the simulation. One thing to note is that the air density used in this simulation is the density of dry air at 1 atm and an ambient temperature of 30°C. Once the initial setup is complete in ANSYS Fluent, Hybrid Initialization is used to initialize all solution variables for the calculation and allow the creation of solution animations. Three solution animations were created: Velocity animation, which visualizes the velocity of air flow along the PVT Collector system on a cross-sectional slice of the system; PV Module Temperature, which visualizes the temperature changes of PV module over time; and Outlet Temperature, which visualizes the temperature changes at the air flow outlet of the PVT collector system, and with all of the settings and initialization done, calculation for the performance of each geometrical design can be done. Calculation settings are left as is, and the number of iterations is set to 100 for each airflow velocity interval. The number of iterations is 100 because the results converge around that number. In other words, the result from each iteration stabilizes, and the difference between each iteration's results becomes negligible, which means that further simulation often does not lead to an improvement in the accuracy or the precision of the simulation.

2.5. Equations and manual calculations

For the CFD simulation and analysis of the five geometrical designs, the only two variables whose values are manually altered are the airflow velocity and the solar irradiance; all other necessary variables either have fixed values or are calculated based on the two manually entered variables and the fixed variables.

With the air flow velocity determined, it is possible to obtain the air mass flow rate via the formula below [22]:

$$\dot{m} = \rho A V \tag{1}$$

where ρ is the density of the fluid (air), V is the flow velocity, and A is the cross-sectional area.

With the mass flow rate calculated, the next step is to calculate the viscosity of air (μ), which determines the air's resistance to flow due to internal friction, and the Reynolds number, which is a number that can be used to predict whether the flow would be laminar or turbulent.

The formulae for the viscosity of air and the Reynolds number are shown below:

$$\mu = [1.983 + 0.00184\ (T_{PV} - 300)] \times 10^{-5} \tag{2}$$

$$\text{Reynolds number} = \frac{\dot{m} D_h}{W . d_\mu} \tag{3}$$

And the hydraulic head (D_h), which is used to calculate the Reynolds number, is calculated with the formula below [23]:

$$Dh\ = \frac{4Wd}{2(W + d)} \tag{4}$$

where T_{PV} is the PV module temperature, W is the width of the channel, and d is the depth of the channel.

To calculate the photovoltaic efficiency (η_{elec}) of the solar photovoltaic thermal system, the following formula relating the photovoltaic efficiency to the maximum power and panel area can be used:

$$\eta_{elec} = \frac{P_{max}}{I\ \times\ A_c} \tag{5}$$

where, P_{max} is the maximum power, I is the solar irradiance, and A_c is the collector area. P_{max} can be calculated with the following formula:

$$P_{max}\ =\ IA_c\alpha_{PV}P(\eta_{PV})\ +\ IA_c\tau_i(1\ -\ P)n_r\alpha_{PV}P(\eta_{PV}) \tag{6}$$

where α_{PV} is the PV temperature coefficient, P is the fraction of irradiance absorbed directly by the semiconductor, η_{PV} is the intrinsic PV conversion efficiency, and τ_i is the optical transmittance.

As for the steps to calculate thermal efficiency, the specific heat capacity of air (C_p) and the rate of heat transfer (Q_u) must first be determined with the linear temperature-dependent specific heat capacity formula for air and the standard energy balance formula shown below [24]:

$$C_p = [1.0057 + 0.000066 \times (T_o - 300)] \times 1000 \tag{7}$$

$$Q_u = \dot{m} C_p (T_o - T_i) \tag{8}$$

where T_o is the outlet temperature, and T_i is the inlet temperature.

With all the necessary variables determined and calculated, the thermal efficiency (η_{th}) can be determined with the formula below [25]:

$$\eta_{th} = \frac{Q_u}{I \times A_c} \tag{9}$$

Finally, with both the photovoltaic efficiency and the thermal efficiency obtained, the two efficiencies can be combined to obtain the overall efficiency of the solar photovoltaic thermal system utilizing a heat-sink fin collector:

$$\eta_{overall} = \eta_{th} + \eta_{elec} \tag{10}$$

3. Results and Discussion

3.1. CFD simulation contour

With the ANSYS Fluent calculation completed, CFD-Post is used to obtain results. A reference plane and line are created at the center of the PVT Collector model to visualize and collect data, as shown in Fig. 6 below. Three contours were created to visualize airflow velocity, PV module temperature, and outlet temperature, and a streamline figure was created to visualize the instantaneous direction and orientation of the airflow. In Fig. 6, the reference plane is shown as the grey plane across the collector system, and the reference line is shown as the yellow line that lies from the center along the reference plane.

Figure 7 shows the velocity along the PVT collector system with colored contours. The contour displayed here is the velocity contour of the first design at an input velocity of 10 m/s, and it is clear that airflow velocity is significantly higher in the channel. The PVT collector system simulated in this project utilizes a model with a double-pass heat dissipation mechanism, where air would enter from the inlet located at the top and flow along the heat sink fins, run into the wall at the end of the collector, and pass through the channel, before eventually flowing along the bottom and exiting the system through the outlet. The high airflow velocity in the channel is caused by the channel being too small for the airflow velocity, creating a bottleneck and resulting in turbulent flow.

Similarly, in Fig. 8, there is significantly more heat around the bottleneck. As the bottleneck limits maximum airflow and causes turbulent flow, a majority of the heat around the bottleneck cannot be dissipated effectively. However, this problem can be easily resolved by increasing the channel's size to make sure airflow is not bottlenecked.

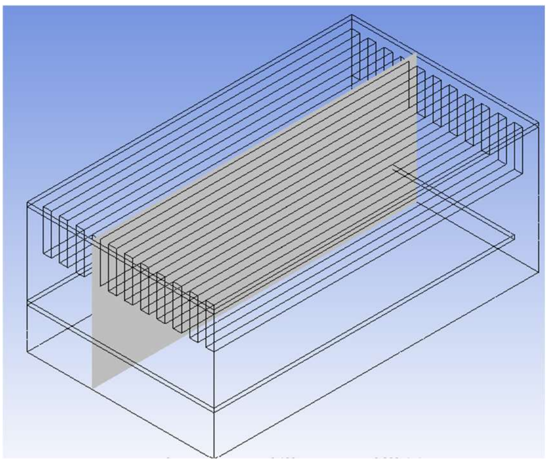

Fig. 6. Reference plane and line in ANSYS CFD-Post.

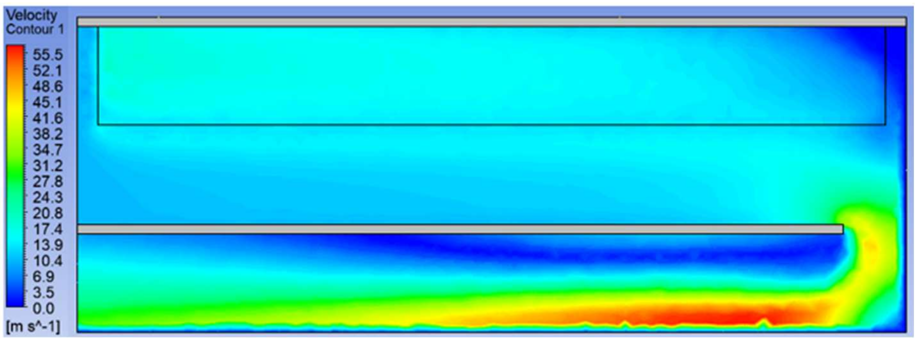

Fig. 7. Airflow velocity contour in ANSYS CFD-Post.

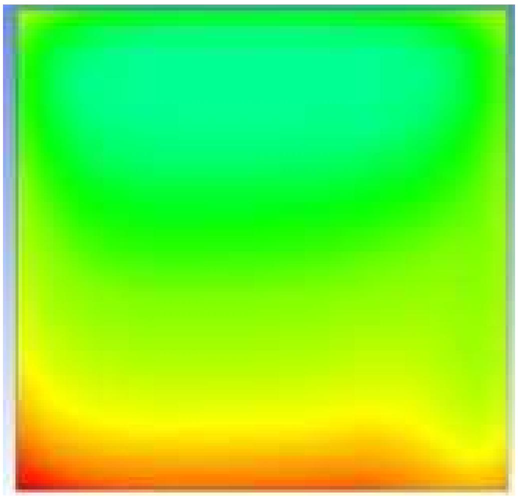

Fig. 8. PV module temperature contour in ANSYS CFD-Post.

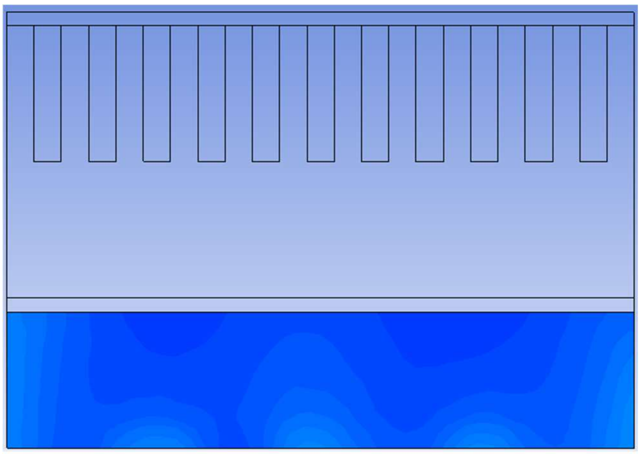

Fig. 9. Outlet temperature contour in ANSYS CFD-Post.

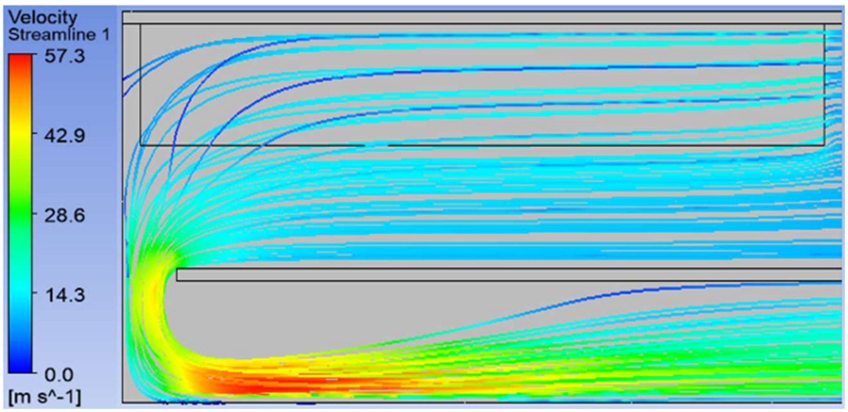

Fig. 10. Air flow streamline in ANSYS CFD-Post.

It can also be seen in Fig. 9 that the temperature contour of the outlet shows that the average temperature of the outlet is around 27~28 degrees Celsius, which could indicate that the PVT collector system does not reach its heat dissipation potential, as the outlet temperature is very close to the ambient temperature of 30 degrees Celsius. Figure 10 shows the airflow, and it becomes apparent that turbulent flow occurs in the bottom half of the PVT collector system due to the bottleneck, with significantly higher airflow velocity in certain sections of the collector. The turbulent flow must be eliminated to ensure heat dissipates in the PVT collector system.

Finally, after all the figures above had been obtained, the function calculator was used to calculate the average temperature along the PV Module and the Outlet. The same process was applied to all five designs, and each airflow velocity was tested. Data obtained from the simulation were recorded and tabulated in Microsoft Excel, where further comparison and analysis were performed, and the best-performing design was determined by comparing electrical and thermal efficiency, which were calculated in Microsoft Excel. Once the best-performing design has been determined, it is tested again with varying solar irradiance and airflow velocity.

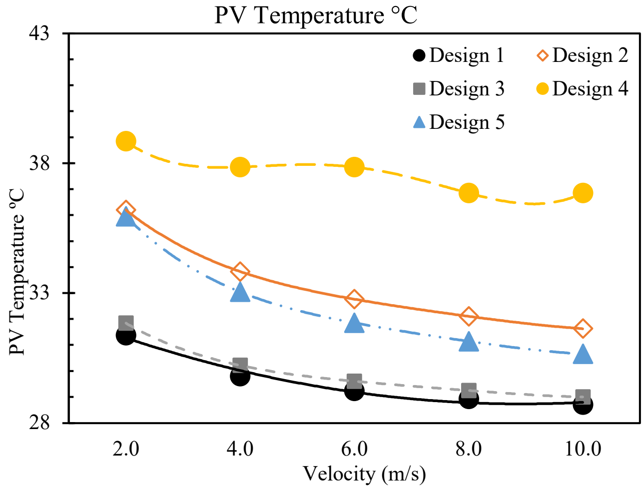

Fig. 11. PV temperature against airflow velocity under constant solar irradiance.

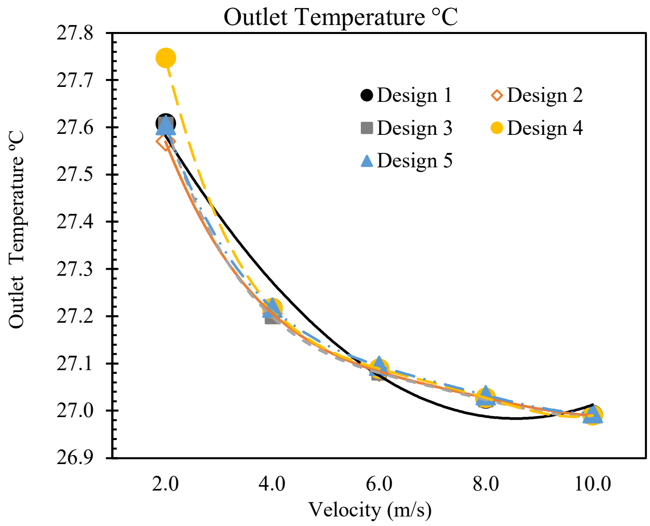

Fig. 12. Outlet temperature against airflow velocity under constant solar irradiance.

3.2. Efficiency comparison of all designs under constant irradiance

The average PV cell temperatures versus inlet air velocity for each of the five designs are plotted in Fig. 11. As seen, the temperature of the cells decreases with increasing air velocity. This is because the higher the airflow is, the greater the convective heat transfer between the PV surface and the cooling air. As velocity increases, the Reynolds number also increases, which decreases the thickness of the thermal boundary layer and increases the convective heat transfer coefficient.

This results in more heat removed from the PV surface and a lower operating temperature. The drop in temperature, however, is less pronounced at increased air velocity. This means that the advantage of the gradual flow rate decreases. The reason is that convective heat transfer approaches the limiting case, in which further decrease in thermal resistance is not very large. The higher the air velocity, the more energy is needed to pump the air, which does not offset the small thermal gain. The results indicate that at a certain level, increasing air velocity peaks the cooling performance, and thereafter the cooling performance does not increase significantly. This means there is an operating range where PVs' energy/thermal efficiency is most efficient.

As with Fig. 11, an increase in airflow velocity decreases the outlet air temperature, as seen in Fig. 12. All cases showed this trend, meaning heat removal improves from the PV system as the flow rate increases. The outlet temperature is not proportional. The rate of decrease declines as airflow velocity increases. This behavior implies that the system tends to move towards a thermally developed condition, and that beyond a certain point, further increases in airflow will result in a decrease in heat transfer. Therefore, it may not be possible to enhance overall system efficiencies by increasing airflow velocity beyond a certain operating range.

It is shown that the PV module temperature and outlet air temperature in Design 1 and Design 3 are the lowest among all the five designs. This trend is also corroborated by PV's efficiency as a function of airflow velocity for all designs, as shown in Fig. 13. As can be seen, design 1 has slightly higher photovoltaic efficiency at lower airflow velocities compared to the other designs at the beginning. Because of its effective thermal regulation, this improvement comes from decreased cell temperature, and the thermal losses in the PV module are kept under control.

As the airflow velocity increases, however, Design 3 gradually outperforms Design 1, as its performance is better at medium- and high-velocity ranges. This behavior implies that at high Reynolds numbers, Design 3's improved convective heat transfer is more apparent, likely due to better flow distribution and air mixing in the channel. However, assessing system performance with PV efficiency alone is not an accurate measure of overall system effectiveness.

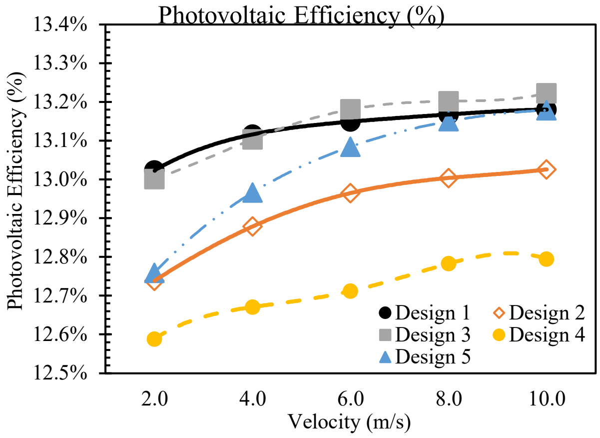

Fig. 13. Photovoltaic efficiency against airflow velocity under constant solar irradiance.

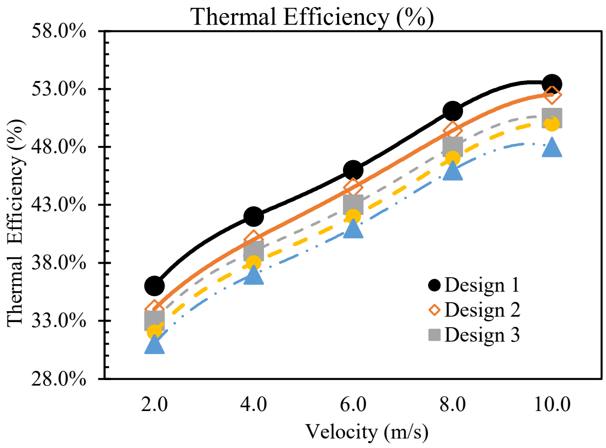

Fig. 14. Thermal efficiency against airflow velocity under constant solar irradiance.

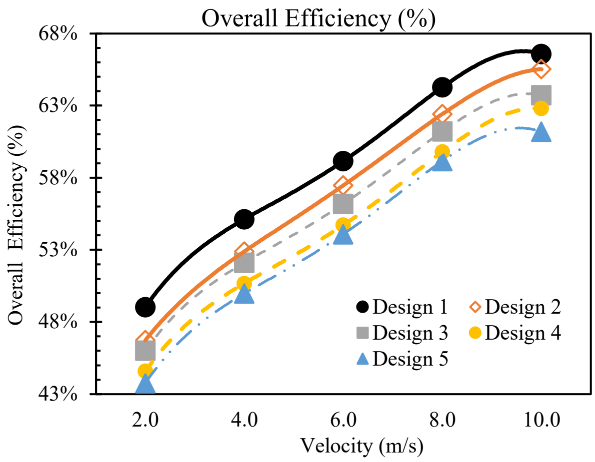

Fig. 15. Overall efficiency against airflow velocity under constant solar irradiance.

Figure 14 shows that the thermal efficiency of Design 3 is relatively low compared to the other designs, showing that less heat is being utilized. Design 1, in contrast, exhibits the best thermal efficiency among the five designs, with a more well-balanced ability to convert/extract thermal energy from the system. This shows that Design 1 is superior in overall thermoelectric performance, whereas Design 3 is superior only based on electrical efficiency under certain operating conditions.

Finally, as each design's performance is determined by its overall efficiency, design 1 is chosen as the best-performing of the five proposed designs, shown in Fig. 15. Although design 3 performs excellently in photovoltaic efficiency, the majority of the overall efficiency is contributed by thermal efficiency. Design 3 is not chosen for further simulation. Based on Figs. 11-15 above, as the airflow velocity increases, both the PV module temperature and outlet temperature tend to decrease. The increase in airflow velocity means more heat can be removed from the PV module, and as the PV module's average temperature decreases, photovoltaic efficiency increases. Thermal efficiency also increases with airflow velocity, as more heat can be carried away in the same amount of time. Therefore, it can be said that as the airflow velocity increases, the overall efficiency of the PVT system utilizing a heat-sink fins collector also increases.

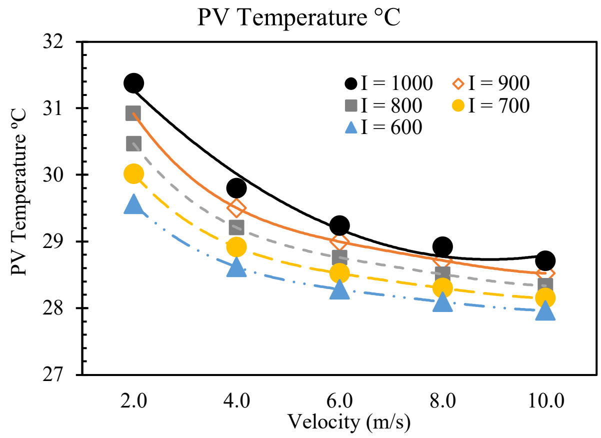

Fig. 16. PV module temperature against airflow velocity under varying solar irradiance.

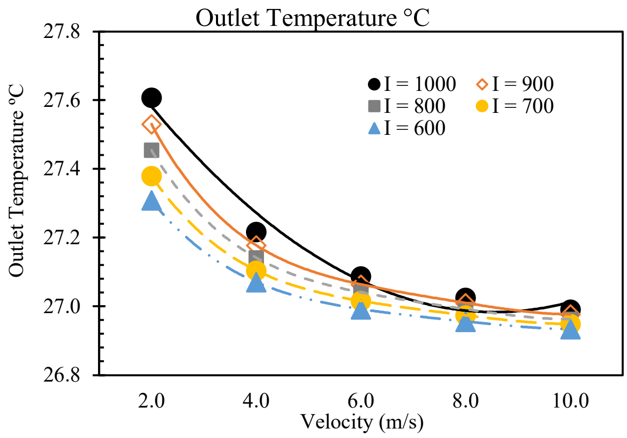

Fig. 17. Outlet temperature against airflow velocity under varying solar irradiance.

Furthermore, based on Fig. 15, design 1 has the best overall efficiency, ranging from 49.02% to 66.58% under constant solar irradiance and varying airflow velocity, with design 2 coming second. Design 1 was chosen for further simulation. A notable mention is design 3, as although it has the highest photovoltaic efficiency, its performance is dragged down by its lower thermal efficiency, which contributes more to the overall efficiency.

3.3. Efficiency of best performing design under varying irradiance

The top-performing design was chosen, and more simulations were run with varying flow speeds and solar intensities. The initial solar irradiance was set to 1000 W/m^2, and decreased in increments of 100 W/m^2 until reaching 600 W/m^2. Figures 16 to 20 show the corresponding results. Figure 16 shows a trend similar to Fig. 11: the average temperature of the PV module decreases as the airflow velocity increases. The relationship follows a logarithmic behavior, meaning that the rate of temperature drop is much higher at lower velocities and decreases as the flow rate increases.

Further, at the same wind velocity, the greater the solar irradiance, the more nearly linear the module temperature increase. This is due to the system's thermal load, storing more heat in the absorber and PV layers. The outlet air temperature as a function of airflow velocity is also shown in Fig. 17 and displays a logarithmic trend. Because of higher convective heat transfer, the outlet temperature drops faster at lower flows, and the rate diminishes at higher flows as the system reaches a thermally developed state. With lower solar irradiance and due to lower cell operating temperature, PV efficiency is slightly higher. The efficiency gap, however, is not significant.

The lowest photovoltaic efficiency is 13.02% at 1000 W/m^2 solar irradiance and 2 m/s airflow velocity, and the highest is 13.13% at 600 W/m^2 solar irradiance and the same airflow velocity. The relatively small difference of 0.11% means that the efficiency difference in the studied irradiance is not large, and the system would not necessarily be near the expected thermal degradation. The thermal efficiency results show an approximately linear dependence on airflow velocity over most of the range studied. At higher velocities around 10 m/s, there is a slight curvature, but the overall trend is relatively linear. This means that higher airflow velocity will further improve the system's heat removal within the investigated velocity range. This near-linear relationship indicates that there are still opportunities to improve the system's heat removal, as full thermal saturation has not yet been achieved with the present operating conditions.

Finally, based on Fig. 20, it can be observed that although the photovoltaic efficiency of design 1 under the solar irradiance of 1000 W/m^2 is the lowest, it did not affect the overall efficiency of the design, as photovoltaic efficiency only contributes to a small fraction of the overall efficiency, meaning that as long as increasing the solar irradiance does not result in a significant drop in photovoltaic efficiency, the overall efficiency of the PVT collector system would increase together with the solar irradiance, and vice versa. Lower solar irradiance means the PVT collector system lacks enough heat exposure, and the airflow does not heat to a desirable temperature, resulting in lower overall thermal efficiency and therefore lower overall efficiency for the PVT system that utilizes a heat-sink fin collector.

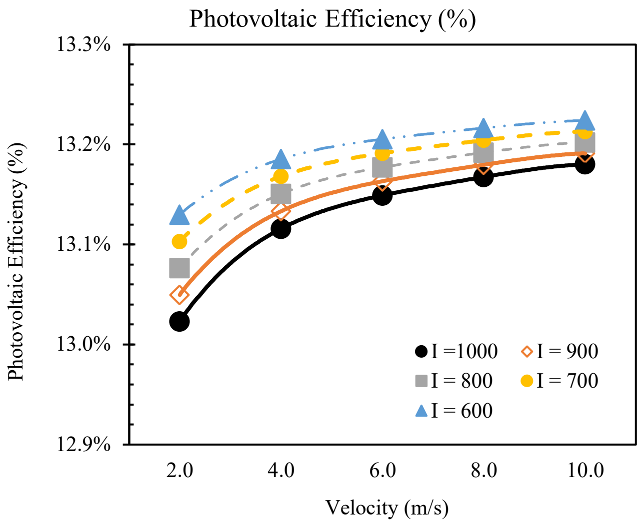

Fig. 18. Photovoltaic efficiency against airflow velocity under varying solar irradiance.

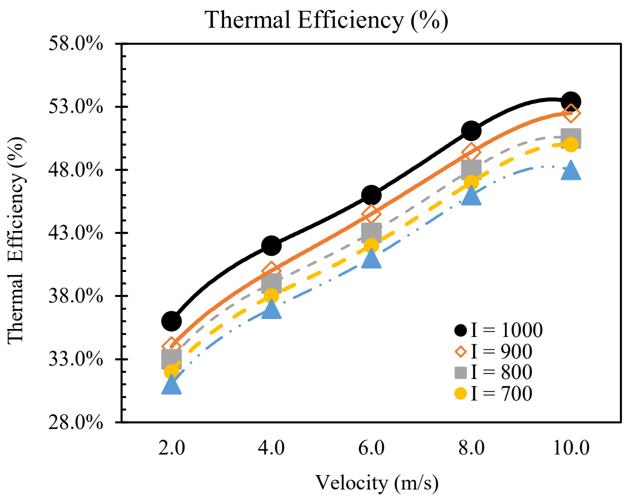

Fig. 19. Thermal efficiency against airflow velocity under varying solar irradiance.

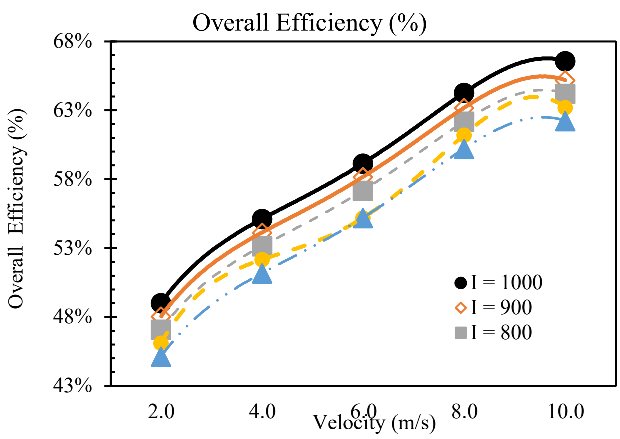

Fig. 20. Overall efficiency against airflow velocity under varying solar irradiance.

4. Conclusion

In conclusion, this paper has established the groundwork for the design, simulation, and optimization of a solar photovoltaic thermal system utilizing a heat-sink fin collector. Using ANSYS Fluent as the CFD analysis software and Microsoft Excel as manual calculation software, simulation and calculation results showed that the proposed designs are feasible, with each design performing at varying efficiencies. From the five designs, Design 1 has the highest overall efficiency, ranging from 45.13% to 66.58% depending on the solar irradiance and airflow velocity. The better performance of Design 1 is due to the high flow disturbance and the heat-transfer surface. Because of flow mixing and the delayed development of the thermal boundary layer, the geometric configuration results in higher convective heat transfer coefficients. The overall efficiency increases with airflow velocity and decreases with solar irradiance.

However, based on outlet temperature and photovoltaic efficiency, the current design of the PVT system with a heat-sink fin collector has not reached its heat-bearing potential. Moving forward, the next step involves further simulation and calculations to investigate the performance of the chosen design under higher solar irradiance and to find an optimal airflow velocity for the highest overall efficiency, while considering the power required for the cooling forced-airflow. This will include repeating the same steps used to obtain the results presented in this paper, this time with much higher solar irradiance to test the performance of the chosen design under high solar irradiance to more closely simulate the average solar irradiance in Malaysia.

The findings of the study can be summarized as follows:

- The results from all five heat sink fin designs showed that design 1 was the most efficient, and the performance range of the design 1 heat sink was from 49.02% to 66.58% under constant solar irradiance conditions.
- The PV module temperature was decreased to less than 30°C, and the air velocity increased from 2 m/s to 10 m/s in the proposed double-pass PVT configuration, which resulted in increased PV efficiency.
- The optimized heat sink fin arrangement showed efficient convective heat transfer enhancement, with photovoltaic efficiencies of around 13.3% and thermal efficiencies of more than 53%.
- It was found that the heat dissipation performance of the system was significantly improved with higher airflow velocity, and lower solar irradiance resulted in a lower thermal contribution of the system.
- The CFD analysis results showed that geometrical modification of heat sinks' fins is a crucial factor in reducing heat accumulation and enhancing the engineering design performance of solar PVT systems.

This comparative analysis will provide critical insights into the practicality and reliability of the proposed design for a solar photovoltaic thermal system utilizing a heat-sink fin collector. Despite satisfactory results from the CFD simulations, there are some noted limitations:

Firstly, the present study involves ANSYS Fluent and numerical simulation, and experimental validation of the proposed designs has not been performed.

Thus, important manufacturing tolerances, material degradation, dust accumulation, and environmental variations were not taken into account. Second, this study focuses on airflow velocity and solar irradiance as the most important parameters; other parameters (i.e., fin thickness, fin spacing, differences in heat sink materials, humidity effects on the fin, and transient weather conditions) were not considered. Besides, the boundary conditions and the collector size used in the present simulation were simplified and may not match large-sized actual operating conditions. The optimized heat sink fin configuration should therefore be subjected to more experimental study under real outdoor operating conditions in the future.

Other optimization studies are also recommended, including using different fin materials, using hybrid fin material, using artificial intelligence for optimization, and using higher ranges of solar irradiance. The geometrical configurations studied in this research are directly applicable to a few, such as heat exchangers, electronic cooling systems, and renewable energy systems like photovoltaic/thermal (PVT) collectors and solar thermal absorbers.

Furthermore, future research could explore the pressure-drop characteristics, forced-airflow power consumption, long-term thermal stability, and techno-economic feasibility to enhance the practical implementation of the proposed double-pass PVT system for larger-scale renewable energy applications.

Author Contributions

L.H. Yang conceptualized the study, developed the methodology, curated the data, and prepared the original draft of the manuscript; M.A.A. Ishak supervised the study, validated the results, conducted the formal analysis, and contributed to reviewing and editing the manuscript; N. 'Atiqah Bt Ahmad conducted the investigation, provided resources, curated the data, and contributed to reviewing and editing the manuscript; Z. Hakiem developed the software, performed the visualization and formal analysis, and contributed to the methodology. The manuscript was written through the contribution of all authors. All authors discussed the results, reviewed, and approved the final version of the manuscript.

Acknowledgments

The authors would like to acknowledge Taylor’s University, University Kebangsaaan Malaysia and University Malaysia Pahang.

Conflict of Interest

The authors declared no potential conflicts of interest concerning the research, authorship, and publication of this article.

Funding

Not applicable.

Data Availability Statements

Not applicable.

References

[1] Zamani, H., Boghrati, M., Hydari, M., Naji-Tabasi, S., Experimental analysis of electrical and solar energy consumption in a hybrid solar flatbread baker, *Solar Energy*, 312, 2026, 114583.
[2] Ishak, M. A. A. Bin, Ibrahim, A., Din, S. I. U., Energy and exergy analysis of a reversed circular flow jet impingement bifacial PVT collector: CFD simulation and experimental study, *Thermal Science and Engineering Progress*, 62, 2025, 103602.
[3] Aziz, M. S. Bin, Ibrahim, A., Ishak, M. A. A. Bin, Energy performance evaluation of a photovoltaic thermal phase change material (PVT-PCM) using a spiral flow configuration, *International Journal of Renewable Energy Development*, 12(5), 2023, 952–958.
[4] Hou, G., Wang, Z., Zhang, Y., Kalogirou, S. A., Markides, C. N., Experimental and numerical investigation of a PVT-PEM system: impact of flow channel configurations on hydrogen production, *Renewable Energy*, 267, 2026, 125741.
[5] Noui, Z., Si-Ameur, M., Bessanane, N., Djebara, A., Ibrahim, A., Ishak, M. A. A. Bin, Ajeel, R. K., Dol, S. S., Comparative study of thermohydraulic performance in mini-channel heat sink systems: Multi-objective optimization and exergy considerations, *Case Studies in Thermal Engineering*, 66, 2025, 105722.
[6] Djebara, A., Bessanane, N., Si-Ameur, M., Ibrahim, A., Al-Tarabsheh, A., Noui, Z., Luqman Azeez, H., Imad ud din, S., Aziat Ishak, A., Performance

evaluation of a Folded heat sink designs for solar cell Cooling: Numerical study, *Thermal Science and Engineering Progress*, 63, 2025, 103724.
[7] Sharma, R. P., Sharma, A., Kumar, V. V., Barik, B. K., Neural network-based predictive model for heat transfer rate in magnetohydrodynamic flow over a stretching cylinder with Cattaneo–Christov heat flux, *Zeitschrift für Angewandte Mathematik und Physik*, 77(2), 2026, 82.
[8] Kumar, V. V., Sharma, R. P., Time-Varying Fluid Injection Mechanism and Enhancing Wall Dilation for Improved Fluid Flow Performance: A Taguchi-Based L16 Orthogonal Array Optimization, *ZAMM - Journal of Applied Mathematics and Mechanics / Zeitschrift für Angewandte Mathematik und Mechanik*, 106(5), 2026, e70469.
[9] Kumar, V. V., Sharma, R. P., Multi-objective optimization of surface-drag phenomena in coaxial disk systems using machine learning assisted Taguchi based grey relation analysis, *International Journal of Numerical Methods for Heat & Fluid Flow*, 36(5), 2026, 1961–1992.
[10] Sharma, R. P., Kumar, V. V., Sharma, A., Praharaj, S., Barik, B. K., Blood rheology-based analytical framework for time-dependent radiative Jeffrey nanofluid flow modelling using Laplace transform, *International Journal of Numerical Methods for Heat & Fluid Flow*, 2026, 1–27.
[11] Zawawi, M. H., Saleha, A., Salwa, A., Hassan, N. H., Zahari, N. M., Ramli, M. Z., Muda, Z. C., A review: Fundamentals of computational fluid dynamics (CFD), *AIP Conference Proceedings*, 2030(1), 2018, 20252.
[12] Ahmed, A., Fouda, A., Elattar, H. F., Alnamasi, K., Alsharif, A. M. A., Advancing photovoltaic thermal module efficiency through optimized heat sink designs, *Applied Thermal Engineering*, 271, 2025, 126241.
[13] Pathak, S. K., Sharma, P. O., Goel, V., Bhattacharyya, S., Aybar, H. Ş., Meyer, J. P., A detailed review on the performance of photovoltaic/thermal system using various cooling methods, *Sustainable Energy Technologies and Assessments*, 51, 2022, 101844.
[14] Pujol, T., T'Jollyn, I., Massaguer, E., Massaguer, A., Cózar, I. R., De Paepe, M., Design optimization of plate-fin heat sink with forced convection for single-module thermoelectric generator, *Applied Thermal Engineering*, 221, 2023, 119866.
[15] Khudhur, D. S., Al-Zuhairy, R. C., Kassim, M. S., Thermal analysis of heat transfer with different fin geometry through straight plate-fin heat sinks, *International Journal of Thermal Sciences*, 174, 2022, 107443.
[16] Harris, M., Wu, H., Angelopoulou, A., Zhang, W., Hu, Z., Xie, Y., Heat transfer optimisation using novel biomorphic pin-fin heat sinks: An integrated approach via design for manufacturing, numerical simulation, and machine learning, *Thermal Science and Engineering Progress*, 51, 2024, 102606.
[17] Chander, S., Purohit, A., Sharma, A., Arvind, Nehra, S. P., Dhaka, M. S., A study on photovoltaic parameters of mono-crystalline silicon solar cell with cell temperature, *Energy Reports*, 1, 2015, 104–109.
[18] Rostami, S., Ibrahim, A., Ishak, A. A., Fazlizan, A., Fudholi, A., Sopian, K., Dehghani-Sanij, A., Shahsavar, A., Al-Aribe, K. M., Experimental and numerical assessment of water-based photovoltaic/thermal collectors with varied tubular absorber cross-sections, *Case Studies in Thermal Engineering*, 65, 2025, 105665.
[19] Gaikwad, A., Sathe, A., Sanap, S., A design approach for thermal enhancement in heat sinks using different types of fins: A review, *Frontiers in Thermal Engineering*, 2, 2023, 980985.
[20] Al-Damook, A., Kapur, N., Summers, J. L., Thompson, H. M., Computational design and optimisation of pin fin heat sinks with rectangular perforations, *Applied Thermal Engineering*, 105, 2016, 691–703.
[21] Yusaidi, N. J., Fauzan, M. F., Abdullah, A. F., Ibrahim, A., Ishak, A. A., Theoretical and experimental investigations on the effect of double pass solar air heater with staggered-diamond shaped fins arrangement, *Case Studies in Thermal Engineering*, 60, 2024, 104619.
[22] Amir, M., Bin, A., Al-aribe, K. M., Aqil, M., Rahmat, A., Imad, S., Din, U., Singh, A., Honeycomb checkered fins Photovoltaic Thermal (PVT): Numerical analysis and experiment validation, *Case Studies in Thermal Engineering*, 75, 2025, 107095.
[23] Ishak, M. A. A. Bin, Ibrahim, A., Fauzan, M. F., Fazlizan, A., Ewe, W. E., Kazem, H. A., The effect of a reversed circular jet impingement on A bifacial module PVT collector energy performance, *Case Studies in Thermal Engineering*, 52, 2023, 103752.
[24] Din, S. I. U., Ibrahim, A., Ajeel, R. K., Fazlizan, A., Ishak, A. A., Al-Aasam, A. B., Thermal performance analysis of a double-pass solar air heater with lava rock as porous and sensible heat storage material, *Journal of Energy Storage*, 95, 2024, 112564.
[25] Alzoubi, M. A., Ibrahim, A., Alkhedher, M., Azeez, H. L., Amir, M., Ishak, A., El Alami, Y., Fazlizan, A., Experimental investigation of energy and exergy characteristics of a novel solar collector with swirling reversed circular flow jet impingement, *Scientific Reports*, 16, 2026, 6812.

ORCID iD

Muhammad Amir Aziat Ishak https://orcid.org/0000-0002-0618-8353
Nurul 'Atiqah Bt Ahmad https://orcid.org/0000-0002-9027-2047
Zikrul Hakiem https://orcid.org/0000-0001-6640-3898

How to cite this article: Yang L.H., et al., Advanced Heat Sink Fin Design: A Study on Geometric Parameters and Their Influence on Convective Heat Transfer for Double-Pass Solar Photovoltaic Thermal (PVT), *J. Appl. Comput. Mech.*, xx(x), 2026, 1–13. https://doi.org/10.22055/jacm.2026.49256.5843